

TR-2009-05

# A Stochastic Approach to Integrated Reliability Prediction

Justin Madsen (jcmadsen@wisc.edu), Dan Ghiocel, David  
Gorsich, David Lamb and Dan Negrut

June 4, 2009

## Abstract

This paper addresses some aspects of an on-going multiyear research project of GP Technologies in collaboration with University of Wisconsin-Madison for US Army TARDEC. The focus of this research project is to enhance the overall vehicle reliability prediction process. A combination of stochastic models for both the vehicle and operational environment are utilized to determine the range of the system dynamic response. These dynamic results are used as inputs into a finite element analysis of stresses on subsystem components. Finally, resulting stresses are used for damage modeling and life and reliability predictions. This paper describes few selected aspects of the new integrated ground vehicle reliability prediction approach. The integrated approach combines the computational stochastic mechanics predictions with available statistical experimental databases for assessing vehicle system reliability. Such an integrated reliability prediction approach represents an essential part of an intelligent virtual prototyping environment for ground vehicle design and testing.

## Contents

1. Introduction.....	4
2. Operational and Vehicle Description .....	4
2.1 Simulation of Stochastic Operational Environment .....	4
2.2 Vehicle Description .....	8
2.2.1 Steering.....	8
2.2.2 Suspension.....	9
2.2.3 Chassis.....	9
2.2.4 Roll Stabilization .....	9
2.2.5 Powertrain .....	10
2.2.6 Tires .....	10
3. Co-Simulation Environment .....	10
3.1 Vehicle Model .....	10
3.2 Tire Model.....	11
3.3 Road Model.....	13
3.4 Event Builder/Driver Controller.....	15
3.5 Batch Simulation Method .....	16
4. Reliability and Life Prediction .....	16
4.1 Subsystem Stress Analysis.....	16
4.2 Progressive Damage and Life Prediction.....	18
5. Selected Results.....	19
5.1 Vehicle Dynamics.....	20
5.2 Stochastic FE Stress Analysis for Left-Front Suspension Subsystem.....	25
5.3 Stochastic Life Prediction .....	27
6. Conclusions.....	30
7. Acknowledgements .....	30
8. References.....	30

# 1. Introduction

This paper addresses some aspects of an on-going multiyear research project of GP Technologies in collaboration with University of Wisconsin-Madison for US Army TARDEC. The focus of this research project is to enhance the overall vehicle reliability prediction process. A combination of stochastic models for both the vehicle and operational environment are utilized to determine the range of the system dynamic response. These dynamic results are used as inputs into a finite element analysis of stresses on subsystem components. Finally, resulting stresses are used for damage modeling and life and reliability predictions. This paper describes few selected aspects of the new integrated ground vehicle reliability prediction approach. The integrated approach combines the computational stochastic mechanics predictions with available statistical experimental databases for assessing vehicle system reliability. Such an integrated reliability prediction approach represents an essential part of an intelligent virtual prototyping environment for ground vehicle design and testing.

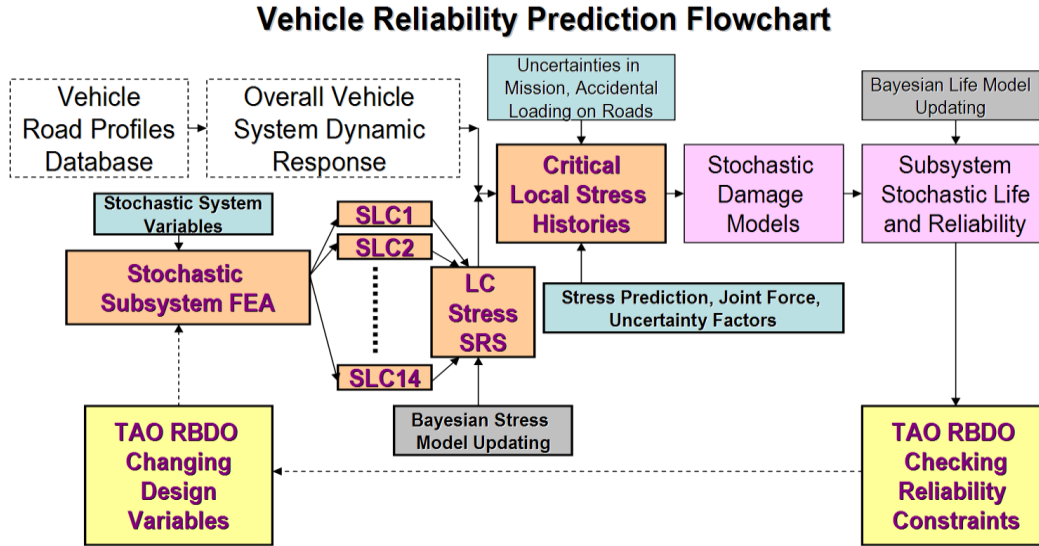


Figure 1: Vehicle reliability prediction flowchart [1]

## 2. Operational and Vehicle Description

This section focuses on the two left-upper boxes in the above reliability chart. We describe the stochastic modeling and simulation of road profiles and corresponding vehicle system dynamic behavior.

### 2.1 Simulation of Stochastic Operational Environment

Stochastic modeling of the vehicle operational conditions includes the following variation components:

- i) stochastic road profiles idealized by a 10 D-1V stochastic vector process with 10 components that describes the statistical road surface amplitude variations on parallel track lines along the road,

ii) stochastic road topography profile idealized by a 1D-3V stochastic vector process with 3 components that describes the statistical variations in 3D space of the slowly varying road trajectory median line

iii) stochastic vehicle chassis speed levels along the road trajectory that include the randomness that is produced by a particular driver's maneuvers for different roughness and topography of road segments, and different drivers' random maneuvers for the same road profile segment.

The idealization of road profiles includes the superposition of two stochastic variations: i) the road surface variation (micro-scale continuous, including smooth variations and random bumps or holes), and ii) the road topography variation (macro-scale continuous variations, including curves and slopes). We assumed that these two stochastic variations are stochastically decoupled, or statistically uncorrelated. We also assume that the road mean surface is horizontal, and therefore no inclination in the transverse direction is considered.

More specifically, we idealized the road surface profiles as non-Gaussian, non-stationary vector-valued stochastic field models with complex spatial correlation structures. To simulate stochastic road profiles, we idealized them by non-Gaussian, non-stationary Markov vector processes that were by solving a set of nonlinearly mapped, stochastically coupled second-order differential equations. The nonlinear mapping is based on an algebraic probability transformation of real, non-Gaussian variations defined by the available databases for road surfaces and topography to an ideal Gaussian image space.

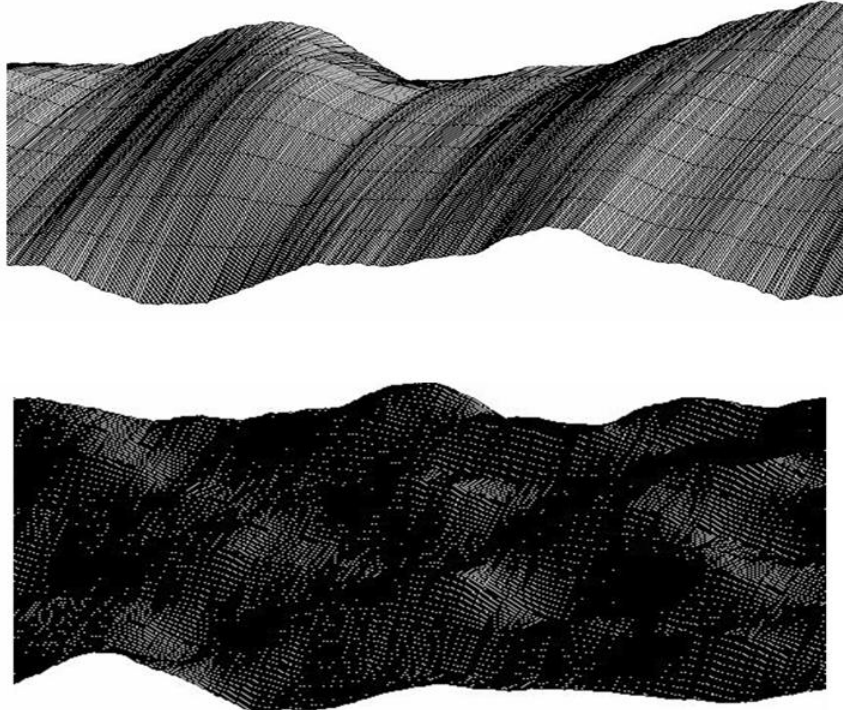


**Figure 2: A simulated road surface with high (top) and low (bottom) spatial correlations. The lateral direction is roughly top to bottom and the longitudinal direction is left to right**

Figure 2 shows simulated road surface segments with high spatial correlation (HC) and low spatial correlation (LC) in the transverse direction of the road. The longitudinal

variation of the mid-line road surface profile is the same for both HC and LC simulated roads. The HC road corresponds to a situation when the wheel inputs are about the same for two parallel wheel lines, so that right-side and left-side wheels see about the same road surface track lines. Thus, for the HC roads, there two different wheel road inputs, each input for a pair of front-rear wheels. In contrast, the LC road assumes that the right-side and left-side wheel road inputs are different. Thus, for LC roads there are four different wheel inputs. Thus, it is expected that a LC road profile will produce much larger vehicle dynamic responses in all directions, especially in the lateral direction.

Based on various road measurements we noted that the road surface variations are highly non-Gaussian as shown in Figure 3. This is somehow surprising for the vehicle engineering community since, traditionally, the road surface profiles have been idealized by simple zero-mean one-dimensional Gaussian stationary stochastic processes. For this type of stochastic processes, only the covariance function (CF), or, alternatively, the power spectral density function (PSD) has to be known to fully describe the road profile. In current practice, the RMS value (equal to the standard deviation of the signal amplitude) and the PSD estimate are often used. Unfortunately, the RMS and PSD estimates are not sufficient for describing non-Gaussian road surface variations as we see from real measurements.

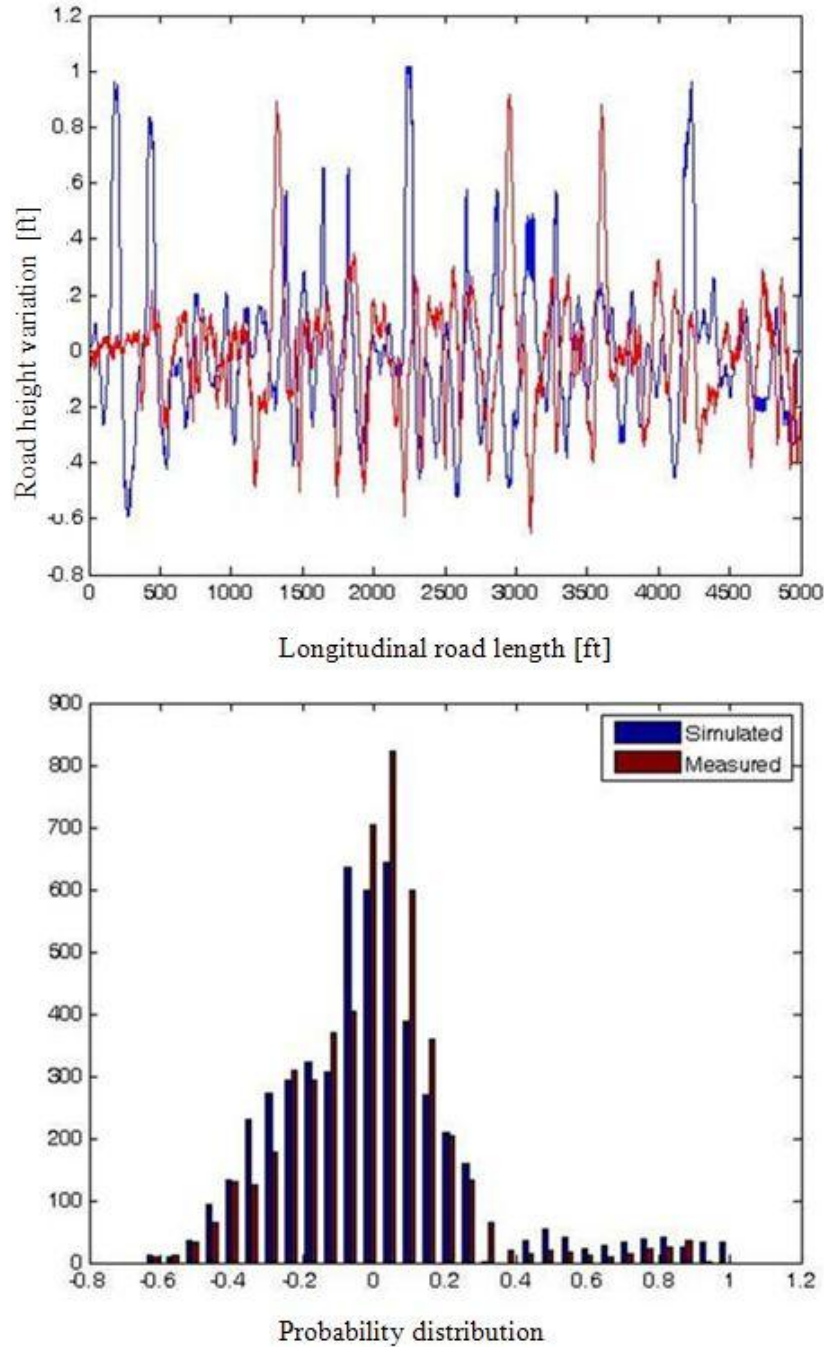


**Figure 3: Simulated and measured road profile variations; Amplitude variations (top) and PSD (bottom)**

We are highly confident that by considering the non-Gaussian variation aspects of road surface variations we are making an important step forward in stochastic modeling of road surface and topography profiles.

It should be noted that the road surface variation is typically highly non-Gaussian, being highly skewed in the direction of large positive amplitudes. Without any doubt, the non-Gaussian variation aspect has a significant negative impact on the vehicle fatigue

reliability. If the non-Gaussian aspects of road surface variations are neglected, the predicted vehicle fatigue life and reliability are much larger than in reality.

## 2.2 Vehicle Description

This project uses the U.S. Army's High-Mobility Multipurpose Wheeled Vehicle (HMMWV) for all dynamic analysis simulations. Specifically, model number M966 (TOW Missile Carrier, Basic Armor without weapons) was selected since values of the total vehicle inertia were available [2].

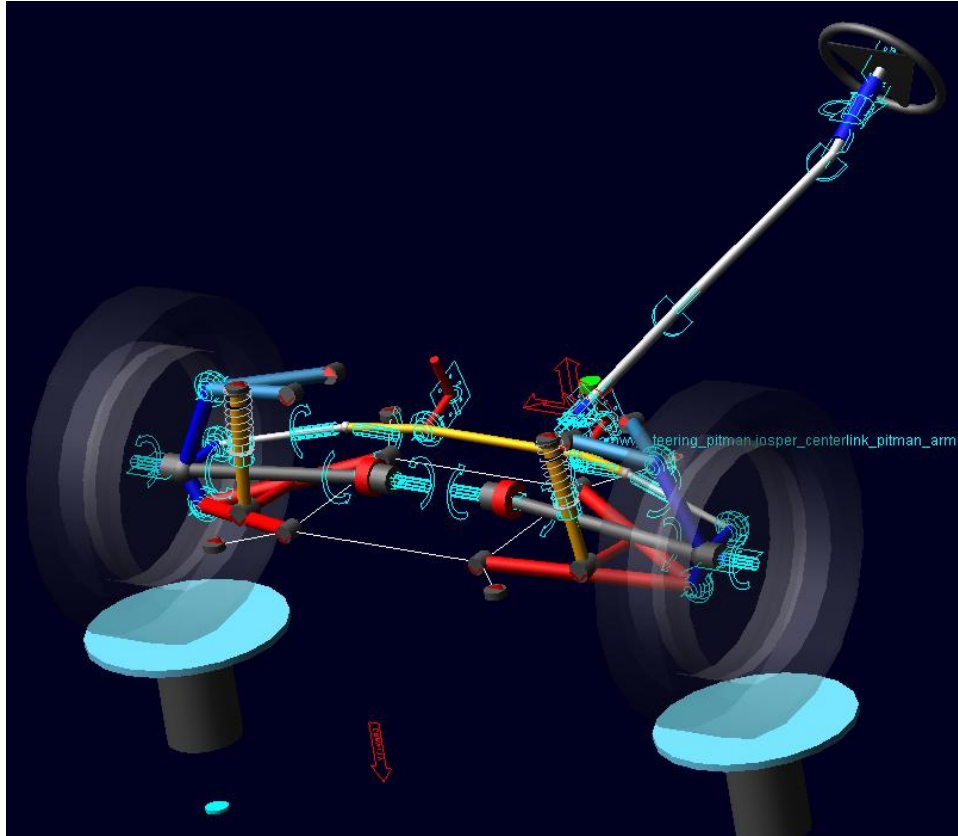


Figure 4: Steering and suspension subsystem models

The vehicle is designed for both on-road and off-road applications, and all models share a common chassis with 4x4 wheel drive that is powered by a 145-hp engine. Only the major subsystems which were included in the dynamic model will be described, which include: parallel link steering with a pitman arm, double A-arm suspension, chassis, roll stabilization bar, powertrain and tires. Subsystems for the brakes and wheels were also included in the multi-body model but will not be described due to their minor role in the simulations.

### 2.2.1 Steering

The HMMWV utilizes a power-assisted parallel link steering system. A pitman arm transfers the steering inputs from the steering wheel to the steering link through a recirculating ball, worm and nut device with a 13/16:1 gear ratio. An idler arm keeps the steering link at the desired height, and tie rods transmit the steering input to the upright



arms located in the suspension subsystem. Topology of the steering system as modeled in the software can be seen with the suspension and wheels in Figure 4.

### **2.2.2 Suspension**

A double Ackerman Arm type suspension unit is used on the HMMWV, one for each wheel. Dimensions and locations of the suspension elements differ between the front and rear subsystems; however, the topology remains the same. Both upper and lower control arms are connected to the upright arm with ball joints. The upright arm connects the wheel spindle to the suspension units. Rear radius rods are connected between the chassis to the rear suspension and control the rear wheel static toe angle. Front tie rods attach the steering subsystem with the front suspension and control the wheel steer angle. Front and rear suspensions both have a design Kingpin angle of 12 degrees and a kingpin offset of 2.14 inches. The front suspension has a caster angle of 3 degrees and a caster offset of 0.857 inches. Topology of the suspension as modeled using virtual prototyping software can be seen in Figure 4.

Shock absorber units are located on each suspension unit, and are attached between the lower control arm and chassis. Each shock absorber is comprised of three elements: a spring, a damper and a bumpstop. At design load and height, the springs are assumed to have linear behavior. The dampers, on the other hand are meant to provide dissipative forces and are not linear. Dissipative forces are proportional to the relative velocity between the piston and cylinder of the shock. Both front and rear springs and dampers were modeled in a similar way, but using different data. The rear springs and dampers are designed for larger operating loads. Bumpstops are located on the end of the damper and provide an additional damping force in the shocks. They are engaged only after a certain amount of displacement occurs between the piston and cylinder of the shock absorber. Spring, damper and bumpstop parameters can be found in [2].

### **2.2.3 Chassis**

The vehicle body is modeled as a single rigid-body component with mass-inertia properties as given in [2]. As stated earlier, both the vehicle mass-inertia properties and the masses of the individual subsystems are known. Simplified geometry like that in Figure 4 was used to calculate each subsystem's respective moment of inertia values. Subtracting the moment of inertia values of the subsystems from that of the overall vehicle yields the sprung chassis moments of inertia.

### **2.2.4 Roll Stabilization**

Auxiliary roll stiffness is provided by an anti-roll bar that is present only in the front suspension and is attached between the lower control arms. Suspension roll is defined as the rotation of the vehicle's sprung mass about the fore-aft centerline with respect to a transverse axis that passes through the left and right wheel centers. Given a suspension roll angle, the anti-roll bar provides an auxiliary roll stabilization force on each lower control arm. The roll bar is modeled as a torsional spring and the torque is assumed to increase linearly with respect to the roll bar twist angle.

### **2.2.5 Powertrain**

The HMMWV is powered by a 6.5L V-8 diesel engine that is rated at 145-hp. An engine map controls the torque at various engine speeds [3] and reaches its maximum torque at 1600 rpm. Engine torque is transferred through a clutch to the 4-speed automatic transmission. Power is then transferred through the differential, and a roughly equal amount of power is transferred to each wheel.

### **2.2.6 Tires**

Tires used for all simulations were the bias-type 36x12.5 LT. Front tire pressures of 20 pounds per square inch (psi) and rear tire pressures of 30 psi were maintained on the HMMWV. By using a tire simulation template modeling scheme, only a select number of tire size, geometry and specification parameters were needed as input into the tire model; other characteristics such as carcass mass/damping/stiffness, tread and friction information were either inherited from the light truck tire template or calculated with a tire simulation pre-processor routine. Details on the tire modeling scheme will be discussed in Section 4.2.

## **3. Co-Simulation Environment**

In light of the importance of the tire/road interaction due to the stochastic modeling of the road profiles, a co-simulation environment was used to accurately capture the vehicle dynamics. ADAMS/Car virtual prototyping software was used to simulate the multi-body dynamics of the vehicle, and the tires and tire/road interaction are simulated by the tire simulation software FTire. Road profiles of nearly a mile in length were used, and as such the computational model for determining the tire/road forces must be efficient and scalable. Parameters used in the vehicle simulation event builder which controls the driver inputs will be discussed. Running each simulation individually was avoided by running large numbers of simulations in batches by using a script to invoke the standalone vehicle model numerous times.

### **3.1 Vehicle Model**

In this work the vehicle simulation software package ADAMS/Car is used to investigate the behavior of the rigid multi-body model of the HMMWV. The modeling methodology divides a vehicle in subsystems that are modeled independently. Parameters are applied to the topology of a subsystem and a set of subsystems are invoked and integrated together at simulation time to represent the vehicle model. The subsystems present in our model include: a chassis, front and rear suspension, anti-roll bar, steering, brakes, a powertrain and four wheels. Note that only the wheels and not the tires are present in the multi-body vehicle model. Also, all the major subsystems (front/rear suspension, steering, roll bar and powertrain) are connected to the chassis with bushing elements. The HMMWV model as seen in the vehicle simulation software is shown in Figure 5 (chassis geometry is partially transparent). CAD geometry is applied to the chassis and tires to make the vehicle look realistic for animation purposes. The geometry has no bearing on the dynamic behavior of the vehicle.

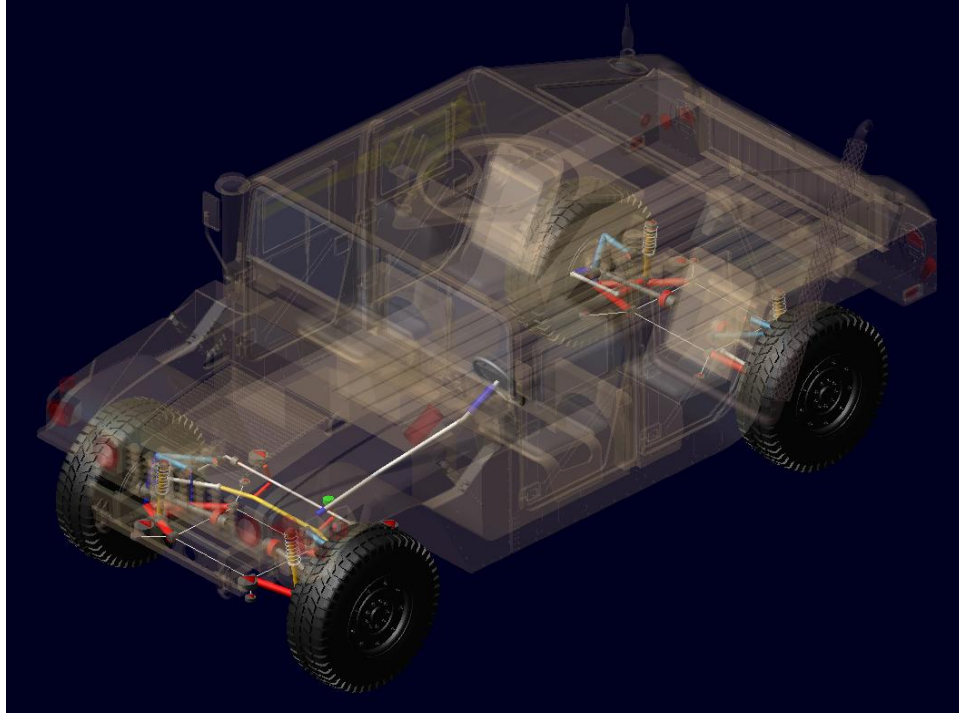
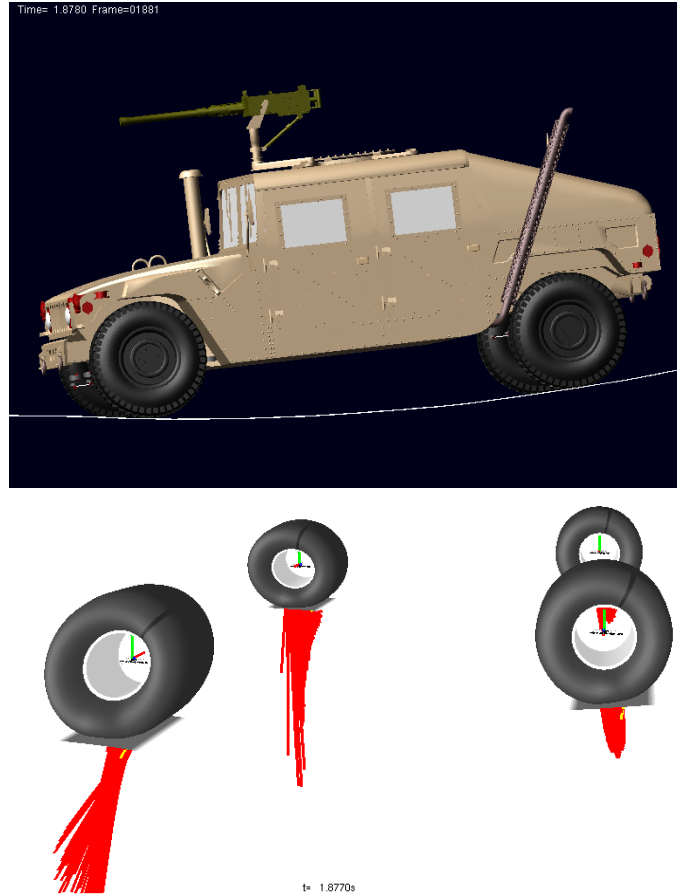


Figure 5: HMMWV model

### 3.2 Tire Model

Due to the variation of the three vehicle operating conditions (micro- and macro-scale road profile variation and vehicle velocity), situations may occur where the vehicle encounters a short-wavelength obstacle at high speed. Therefore, FTire, a robust tire model that can handle these obstacles while undergoing large deflections, was used. Figure 6 gives an example of the vehicle and tire models traversing the exit lip of a hill at moderate speed.



**Figure 6: HMMWV model (top) and tires (bottom) traversing a hill**

As indicated in an example online documentation<sup>1</sup>, the FTire [4] model serves as a sophisticated tire force element. It can be used in multi-body system models for vehicle ride comfort investigations as well as other vehicle dynamics simulations on even or uneven roadways. Specifically, the tire model used is designed for vehicle comfort simulations and performs well even on obstacle wave lengths as small as half the width of the tire footprint. At the same time, it serves as a physically based, highly nonlinear, dynamic tire model for investigating handling characteristics under the above-mentioned excitation conditions [5]. Computationally the tire model is fast, running only 10 to 20 times slower than real time. The tire belt is described as an extensible and flexible ring carrying bending loads, elastically founded on the rim by distributed, partially dynamic stiffness values in the radial, tangential, and lateral directions. The degrees of freedom of the ring are such that both in-plane and out-of-plane rim movements are possible. The ring is numerically approximated by a finite number of discrete masses called belt elements. These belt elements are coupled with their direct neighbors by stiff springs with in- and out-of-plane bending stiffness [4]. Figure 7 illustrates this modeling approach. Each belt element contains a certain number of massless tread blocks which convey the nonlinear stiffness and damping in the radial, tangential and lateral directions. The stiffness and damping values are determined during the pre-processing phase, which are

<sup>1</sup> [http://www.ftire.com/docu/ftire\\_fit.pdf](http://www.ftire.com/docu/ftire_fit.pdf)

fitted to the tire's modal and static properties. Radial deflections of the blocks depend on the road profile and orientations of the associated belt elements, while tangential and lateral deflections are determined using the sliding velocity on the ground. The tire modeling software calculates all six components of tire forces and moments acting on the rim by integrating the forces in the elastic foundation of the belt.

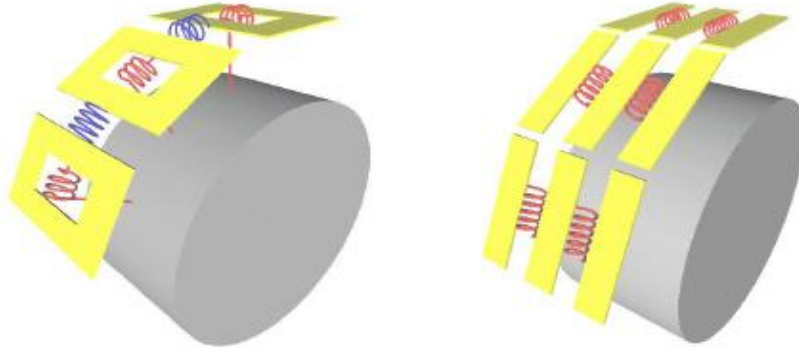


**Figure 7: FTire modeling approach**

Because of this modeling approach, the resulting tire model is accurate up to relatively high frequencies both in longitudinal and in lateral directions. There are few restrictions in its applicability with respect to longitudinal, lateral, and vertical vehicle dynamics situations. It works out of and up to a complete standstill with no additional computing effort or any model switching. Finally, it is applicable with high accuracy in demanding applications such as ABS braking on uneven roadways [5].

### **3.3 Road Model**

The road models supported should run efficiently and accommodate the fidelity level of the tire model. The vehicle simulation uses a road which is defined by a text based road data file (\*.rdf). This file contains the road characteristics such as size, type, profile, friction coefficients etc. The road profile can be defined in a number of ways. In ADAMS/Car, a triangle mesh is generally used to define a road with varying elevation in both the longitudinal and lateral directions. Sets of vertices are grouped to define triangles that make up the mesh. Figure 8 shows a section of road made up of this type of triangle mesh.

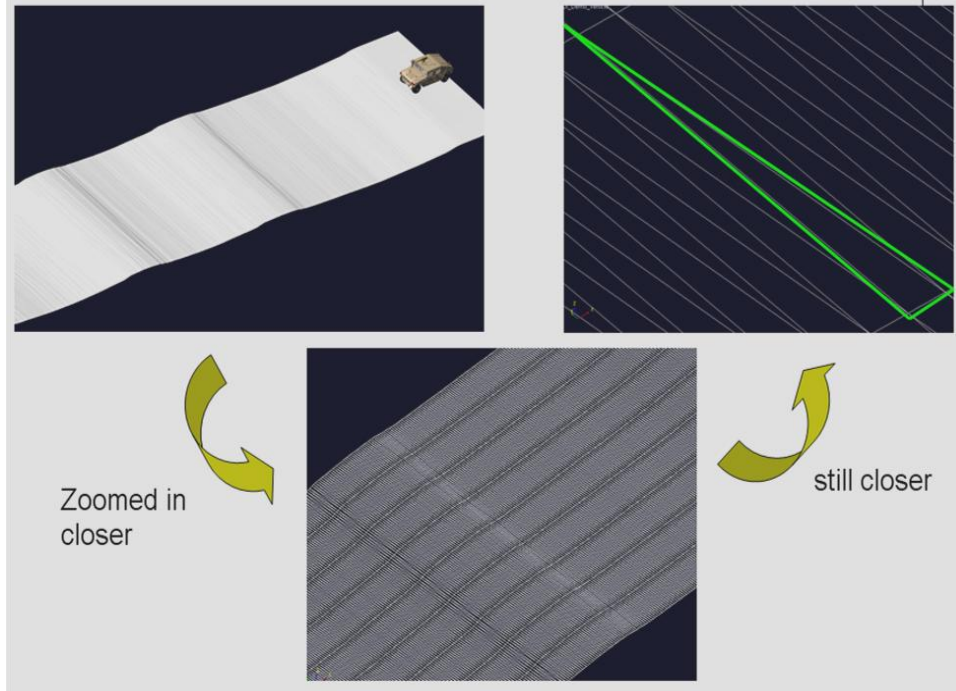


**Figure 8: Road profile defined as a triangle mesh**

Although the level of fidelity can be as high as the total number of known vertices, the simulation time required per time step increases exponentially with the number of triangles in the mesh. It was determined that for each time step, the simulation had to check every triangle for contact with the tire patch. The bottleneck in the simulation was due to the 300,000+ triangles that describe road profiles. In order to simulate large road profiles with high fidelity the tire simulation specific regular grid road (\*.rgr) data file format was selected. Under the assumption that the input road data points are equally spaced in the lateral and longitudinal directions, a conversion from a triangle mesh (\*.rdf) to a regular grid road (\*.rgr) file type is possible. To preserve the accuracy of the road profile, if the spacing between input road data points differs between the lateral and longitudinal directions, the smaller of the two values is used for the size of each grid element. The advantages of using this type of road data file type are that the file size is usually smaller and the CPU time per simulation step is independent of the size or fidelity of the road. The disadvantage is that a conversion is necessary and if incorrect parameters are chosen, the file size can balloon or the accuracy of the road profile can diminish. The similarity between a section of road in both (\*.rdf) and (\*.rgr) file types when conversion parameters are carefully selected can be seen in Figure 9.



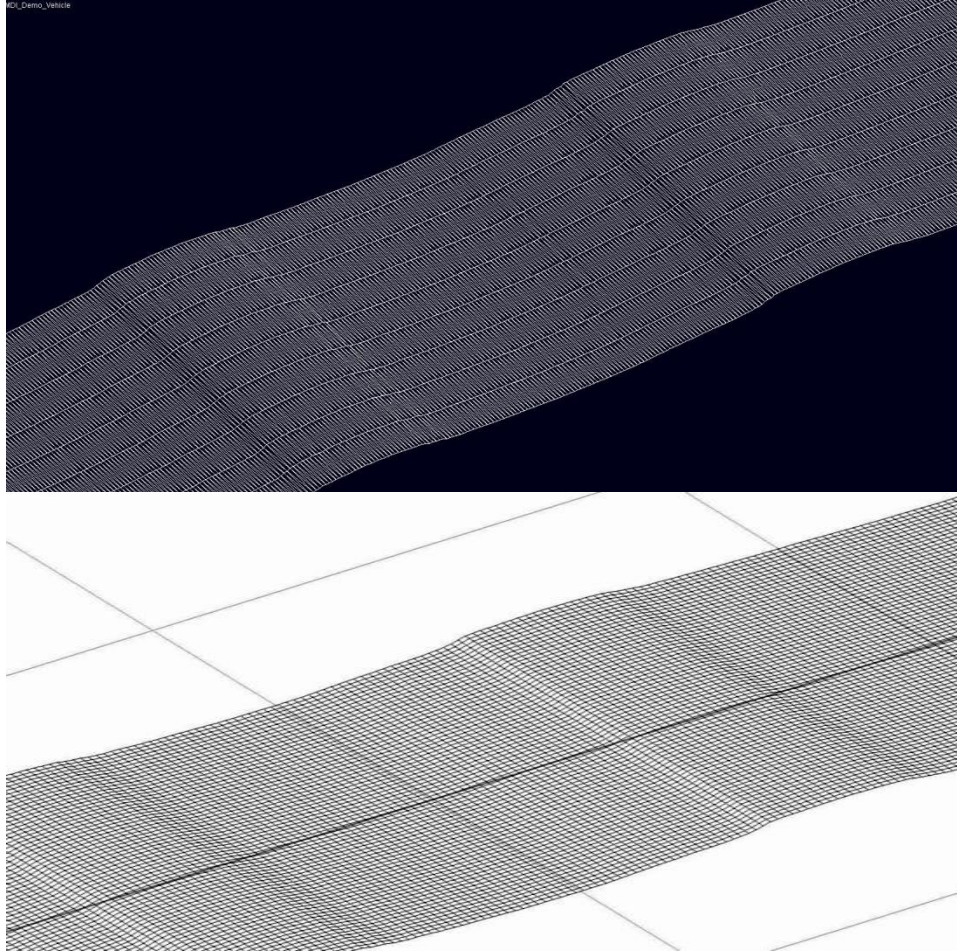


Figure 9: Section of road in vehicle simulation (\*.rdf) format (top) and tire simulation (\*.rgr) format (bottom)

### 3.4 Event Builder/Driver Controller

Driver controls were created in the vehicle simulation software event builder as a sequence of maneuvers. Maneuvers are defined by steering, throttle, brake, gear, and clutch parameters. In this set of simulations, a single maneuver is performed in which the vehicle attempts to follow the centerline of the road profile at a given vehicle speed.

An ADAMS/Car module called the “Driving Machine” utilizes the values that were given as inputs into the event builder and uses driver controls to simulate custom vehicle maneuvers. Steering is controlled by specifying a vehicle path in an external file and actuated by applying a torque on the steering wheel. Engine throttle is controlled with an external file which specifies the vehicle longitudinal velocity at a given position on the road. The braking, gear and clutch all reference the same external file and serve to control the vehicle speed.

Static set-up and gear shifting parameters are not modified; however, the drive authority is sometimes reduced when large obstacles and high vehicle speeds cause simulations to fail. Drive authority specifies how aggressively the vehicle steering torque is applied when the vehicle deviates off the specified path. As the wheelbase of the HMMWV is wide and long, the minimum preview distance was substantially increased from its default value.

### **3.5 Batch Simulation Method**

In light of the large number of stochastic variables to be simulated and analyzed, a scripted batch simulation procedure was embraced. For each simulation, a set of stochastic variables including, road profile, driver control and vehicle parameters are chosen. The vehicle model and operational environment are set up to reflect these choices, then the vehicle simulation solver files are saved for each particular simulation set-up. Large sets of vehicle simulation solver files are created, and a script is then invoked to run the entire set of simulations in the stand-alone solver. The co-simulation environment is automatically invoked, and results files are saved. Vehicle specific information is post-processed and extracted using scripts/macros. Tire specific information is stored in a tire simulation result file, and is post-processed.

## **4. Reliability and Life Prediction**

A parallel computing approach is used handle the large size of the finite-element (FE) models by combining the decomposition in both the physical-model space and sample data space. This allows the problem to be split into FE submodels which can be solved on a single processor. Preconditioners are used to increase the numerical efficiency when solving the finite-element analysis (FEA) problem, especially when the problem is nonlinear. Refined stochastic response surface approximation (SRSA) models are used to compute local stresses in subsystem components.

Once local stress response surfaces are known, a number of stochastic cumulative damage models are considered. Rainflow cycle counting and Neuber's rule for local plasticity modeling were used for any irregular stress-strain histories. Crack propagation and corrosion-fatigue damage effects were also considered and probabilistic life prediction models were based on both lognormal and Weibull probability distributions.

### **4.1 Subsystem Stress Analysis**

The stochastic subsystem stress analysis is based on a efficient high-performance computing (HPC) stochastic FEA code that was developed with support from UC Berkeley. The developed HPC stochastic FEA code is a result of integrating the finite element software FEAP with a number of modules used for stochastic modeling and simulation that run together in an efficient computing environment driven by advanced HPC numerical libraries available from national labs and top universities.

In addition to the standard FEA and HPC algorithms, the FEA code includes a unique suite of computational tools for stochastic modeling and simulation and stochastic preconditioning [1].

For stochastic FEA domain decomposition, an efficient multilevel partitioner software package developed by the University of Minnesota was used. Multilevel partitioners rely on the notion of restricting the fine graph to a much smaller coarse graph, by using maximal independent set or maximal matching algorithms. This process is applied recursively until the graph is small enough that a high quality partitioner, such as spectral bisection or k-way partitioners, can be applied. This partitioning of the coarse problem is then "interpolated" back to the finer graph – a local "smoothing" procedure is then used, at each level, to locally improve the partitioning. These methods are poly-



logarithmic in complexity though they have the advantage that they can produce more refined partitions and more easily accommodate vertex and edge weights in the graph.

The main idea to build a flexible HPC implementation structure for stochastic parallel FEA has been to combine the parallel decomposition in the simulated sample data space with the parallel decomposition in the physical-model space. This combination of parallel data space decomposition with parallel physical space decomposition provides a very high numerical efficiency for handling large-size stochastic FE models. This HPC strategy provides an optimal approach for running large-size stochastic FE models. We called this HPC implementation Controlled Domain Decomposition (CDD) strategy. The CDD strategy can be applied for handling multiple FE models with different sizes that will be split on a different number of processors as shown Figure 10. There is an optimum number of processors to be used for each FE model, so that the stochastic parallel FEA reaches the best scalability. The main advantage of the CDD implementation for HPC FEA is that large-size FE models can be partitioned into a number of FE submodels, each being solved on a single processor. Thus, each group of processors is dedicated to solve a large-size FE model. CDD ensures dynamic load balancing after a group of processors has completed its allocated tasks and it becomes available for helping another group of processors.

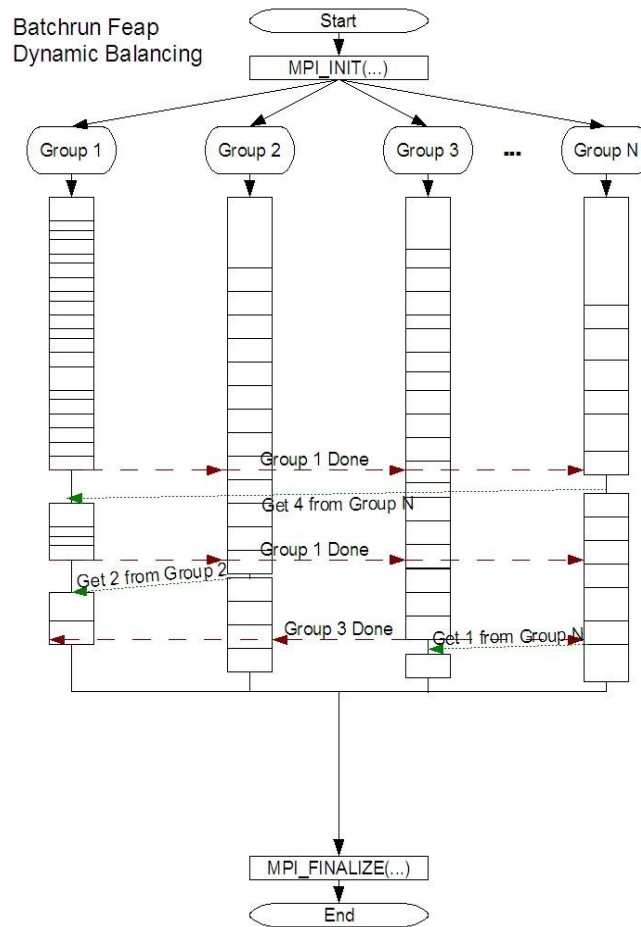


Figure 10: CDD Strategy implementation

To be highly efficient for large-size FEA models, the FEA code incorporates a unique set of powerful stochastic preconditioning algorithms, including both global and local sequential preconditioners. The role of preconditioning is of key significance for getting fast solutions for both linear and nonlinear stochastic FEA problems. It should be noted that the effects of stochastic preconditioning is larger for nonlinear stochastic FEA problems since it reduces both the number of Krylov iterations for linear solving and the number of Newton iterations for nonlinear solving. The expected speed up in the FEA code coming from stochastic preconditioning is at least 4-5 times for linear FEA problems and about 10-15 times for highly nonlinear FEA problems.

To compute local stresses in subsystem components, refined stochastic response surface approximation (SRSA) models are used. These SRSA models are based on high-order stochastic field models that are capable of handling non-Gaussian variations [6-7]. The SRSA implementations were based on two and three level hierarchical density models as shown in Figure 11. It should be noted that these SRSA models are typically more accurate than traditional responses surfaces, and are also limited to the mean response surface approximation.

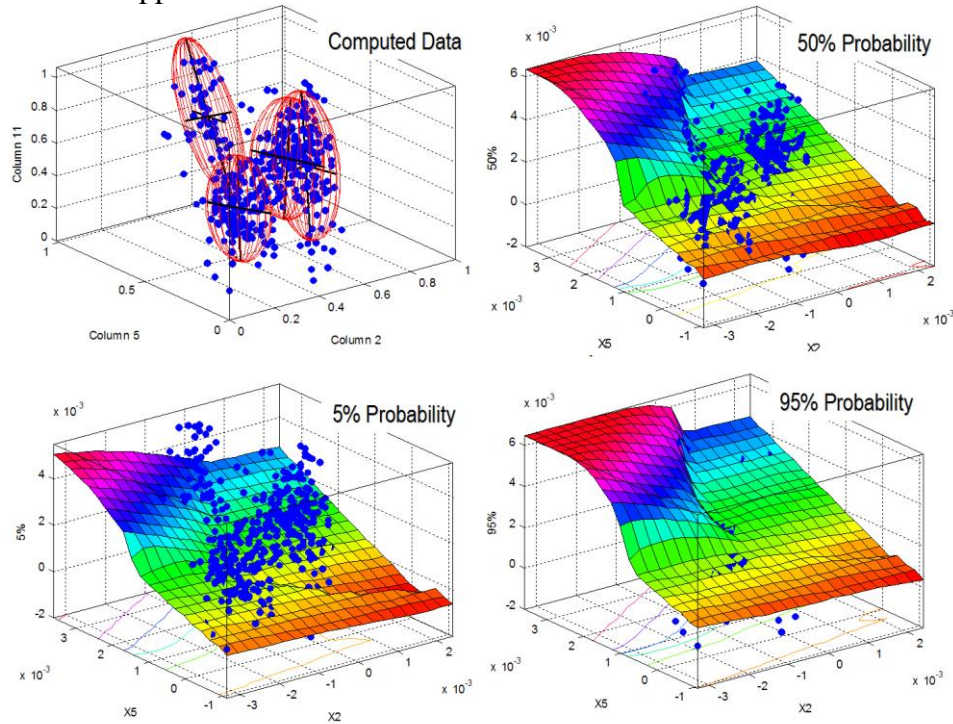


Figure 11: Probability-level response surfaces

## 4.2 Progressive Damage and Life Prediction

For fatigue modeling, the following cumulative damage models are considered:

*Crack Initiation*, Stochastic Phenomenological Cumulative Damage Models:

- 1) Linear Damage Rule (Miner's Rule)
- 2) Damage Curve Approach (by NASA Glenn)
- 3) Double Damage Curve Approach (by NASA Glenn)

### *Crack Propagation, Stochastic Linear Fracture Mechanics-based Models:*

#### 1) Modified Forman Model (by NASA JPC)

Both the constitutive stress-strain equation and strain-life curve are considered to be uncertain. The two Ramberg-Osgood model parameters and the four strain-life curve (SLC) parameters are modeled as random variables with selected probability distributions, means and covariance deviations. We also included correlations between different parameters of SLC. This correlation can significantly affect the predicted fatigue life estimates.

We combined rainflow cycle counting with the Neuber's rule for local plasticity modeling for any irregular stress-strain history. For a sequence of cycles with constant alternating stress and mean stress the Damage Curve Approach (DCA) and Double Damage Curve Approach (DDCA) were implemented. In comparison with the linear damage rule (LDR) or Miner's rule, these two damage models predict the crack initiation life,  $N_f(\epsilon_a, \sigma_m)$  much more accurately. The shortcoming of the popular LDR or Miner's rule is its stress-independence, or load sequence independence. LDR is incapable of taking into account the interaction of different load levels, and therefore interaction between different damage mechanisms or failure modes. There is substantial experimental evidence that shows that LDR is conservative under completely reversed loading condition for low-to-high loading sequences,  $\sum r_i > 1.0$ , and severely under conservative for high-to-low loading sequence,  $\sum r_i < 1.0$ .

For intermittent low-high-low-high-...cyclic loading, the LDR severely underestimates the predicted life. The nonlinear damage models, DCA and DDCA, were implemented to adequately capture the effects of the HCF-LCF interaction and corrosion-fatigue damage for vehicle subsystem components.

Crack propagation was implemented using a stochastic modified Forman model. Both the stress intensity threshold and material toughness are considered as random variables.

Corrosion-fatigue damage effects due to pitting growth were considered by implementing a simultaneous corrosion-fatigue (SCF) model [8]. The total corrosion-fatigue damage in the crack nucleation stage is computed using a generalized interaction curve between corrosion and fatigue damages, while the in crack propagation stage is computed by linear fracture mechanic models (Forman model) for which the stress intensity factors are adjusted based on local crack size including both the fracture crack and the pit depth.

We included probabilistic life prediction models based on both the lognormal and the Weibull probability distributions.

## **5. Selected Results**

The following two sections present examples of results for both the vehicle dynamics and resulting stochastic FE stress analysis. Results of the vehicle encountering two different types of obstacles will be presented and discussed. Results from the stress analysis and the effects of selecting a certain damage rule are shown.

## 5.1 Vehicle Dynamics

Many of the results from the vehicle dynamic simulations are focused on the front-left suspension subsystem (FLSS), although all four tire deflections and gross vehicle behavior were monitored as well. As seen in Figure 6, the vehicle can encounter a wide variety of obstacles. In this particular case, the exit lip of a hill is being traversed while steering around a left-hand corner at moderately high speed. Road/tire forces are represented with red vectors in Figure 6 and it is apparent that this maneuver results in large forces being applied to the front two tires. Figure 12 plots the deflection of the front left tire when the vehicle traverses the obstacle at time = 1.88 seconds. Analysis of subsystem results verifies the large forces experienced by the components in the front left suspension. The reaction forces in the lower control arm ball joint over this time period are plotted in Figure 13. Large vertical reaction forces can be seen when the vehicle encounters the obstacle. The shock spring and bumpstop forces are plotted in Figure 14, and illustrates that the maneuver is severe enough to engage the bumpstop.

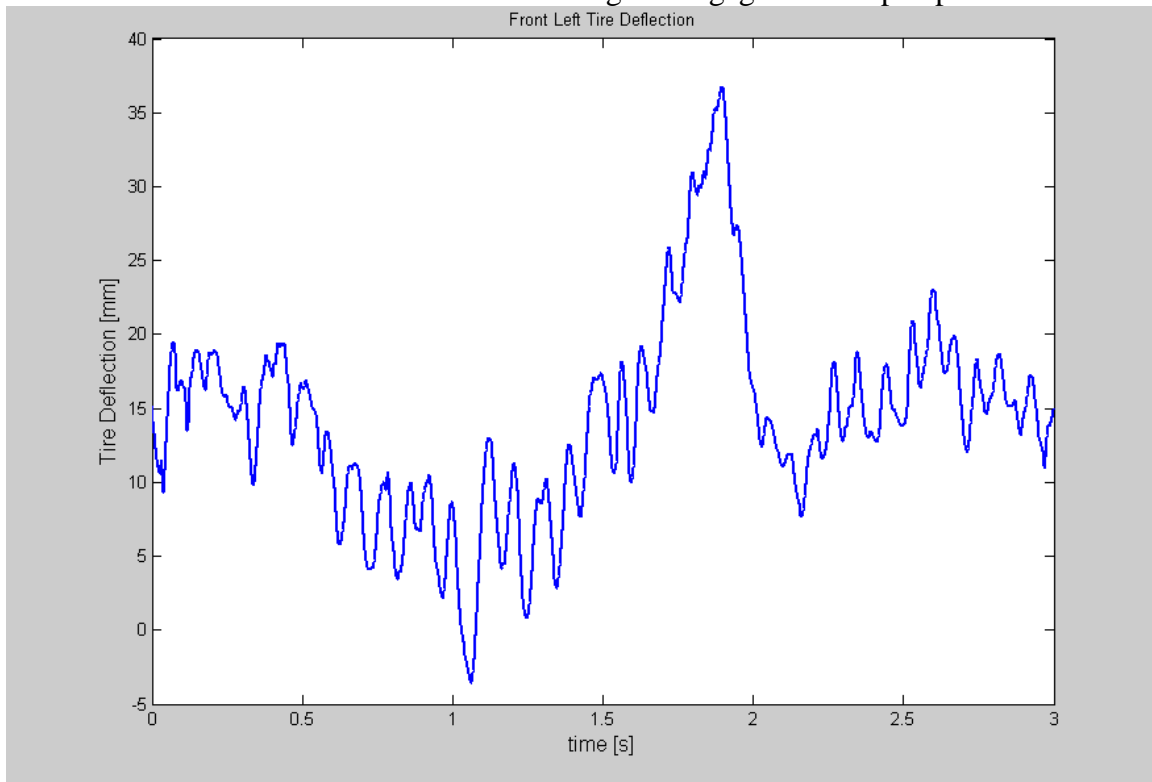


**Figure 12: Front left tire deflection as the vehicle traverses an obstacle**

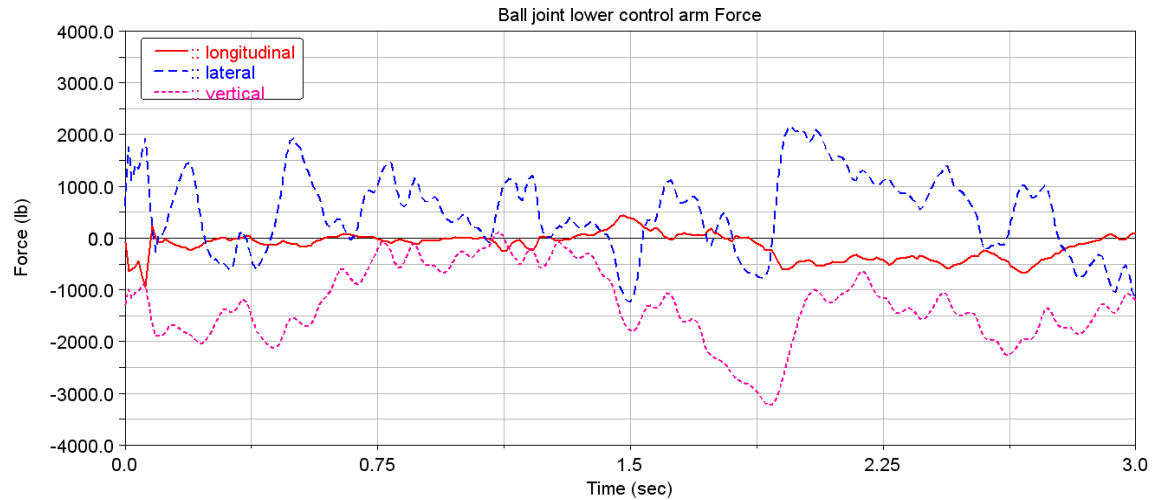


**Figure 13: Large vertical reaction forces in the lower control arm ball joint**

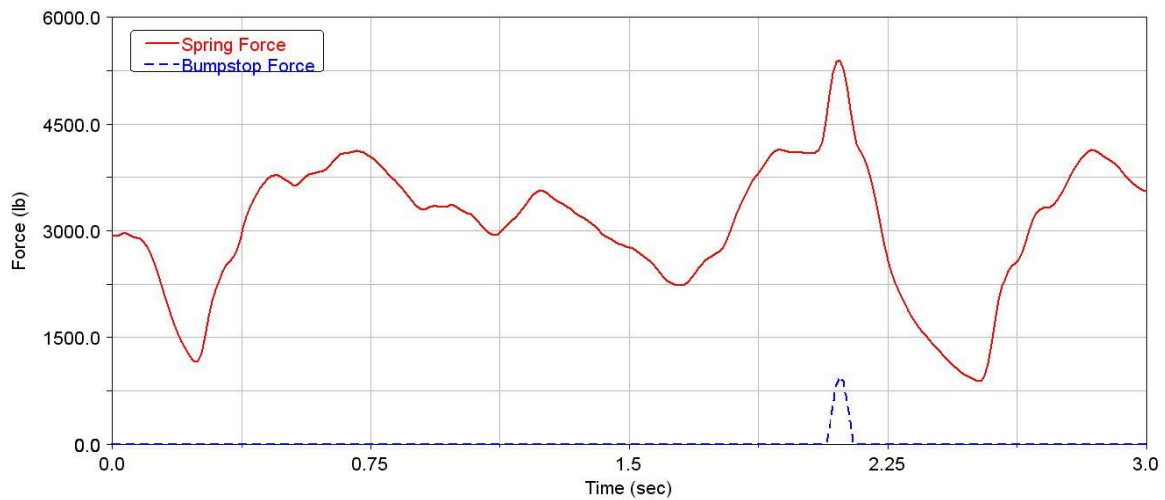


**Figure 14: Spring and bumpstop forces as the vehicle traverses an obstacle**

Effects of the vehicle's speed have a significant impact on the forces in the components, especially when combined with obstacles encountered on rough off-road terrain. At a certain distance along a road profile, the HMMWV encounters a small ditch/pothole type obstacle as seen in Figure 15. The response of the vehicle due to this obstacle was captured at low and high speeds.

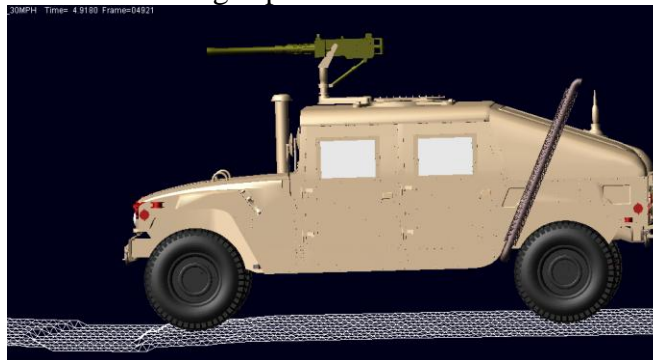


**Figure 15: HMMWV model prior to encountering a pothole obstacle**

Figure 16 shows the spring forces in the front suspension, and it appears that the high-speed case experiences a maximum spring force ~500 lb. larger than the low-speed case. Similar patterns in the spring force lead to the conclusion that the first spike after the dip below the steady state value is caused when the front tires enter the obstacle, and the final and largest spike occurs when the vehicle traverses the exit lip of the obstacle. Figure 17 shows the tire deflection of the front left tire to verify the simulation times at which the vehicle enters and exits the obstacle in Figure 15 for both the low speed and high speed cases.

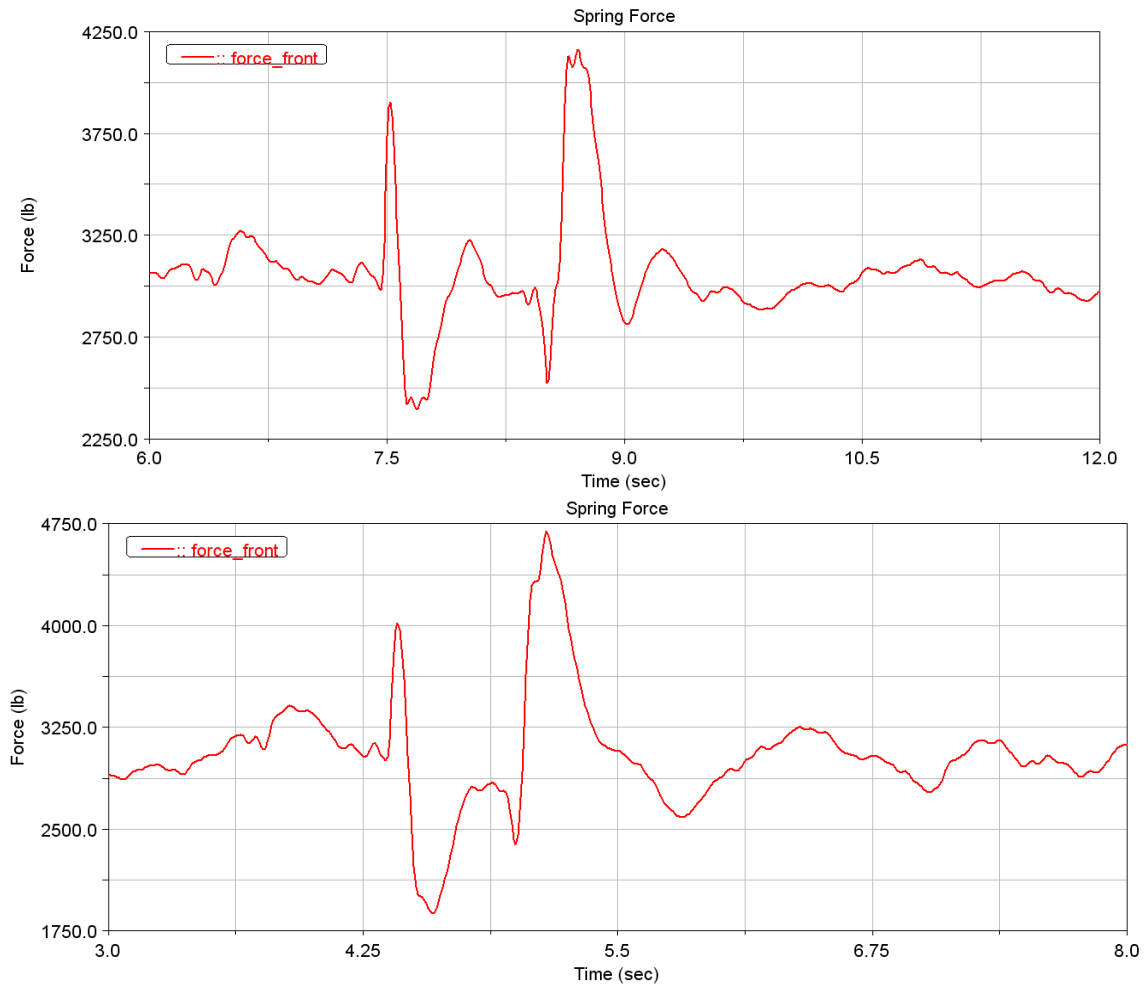


**Figure 16: Spring force, low-speed case (top) and high-speed case (bottom)**

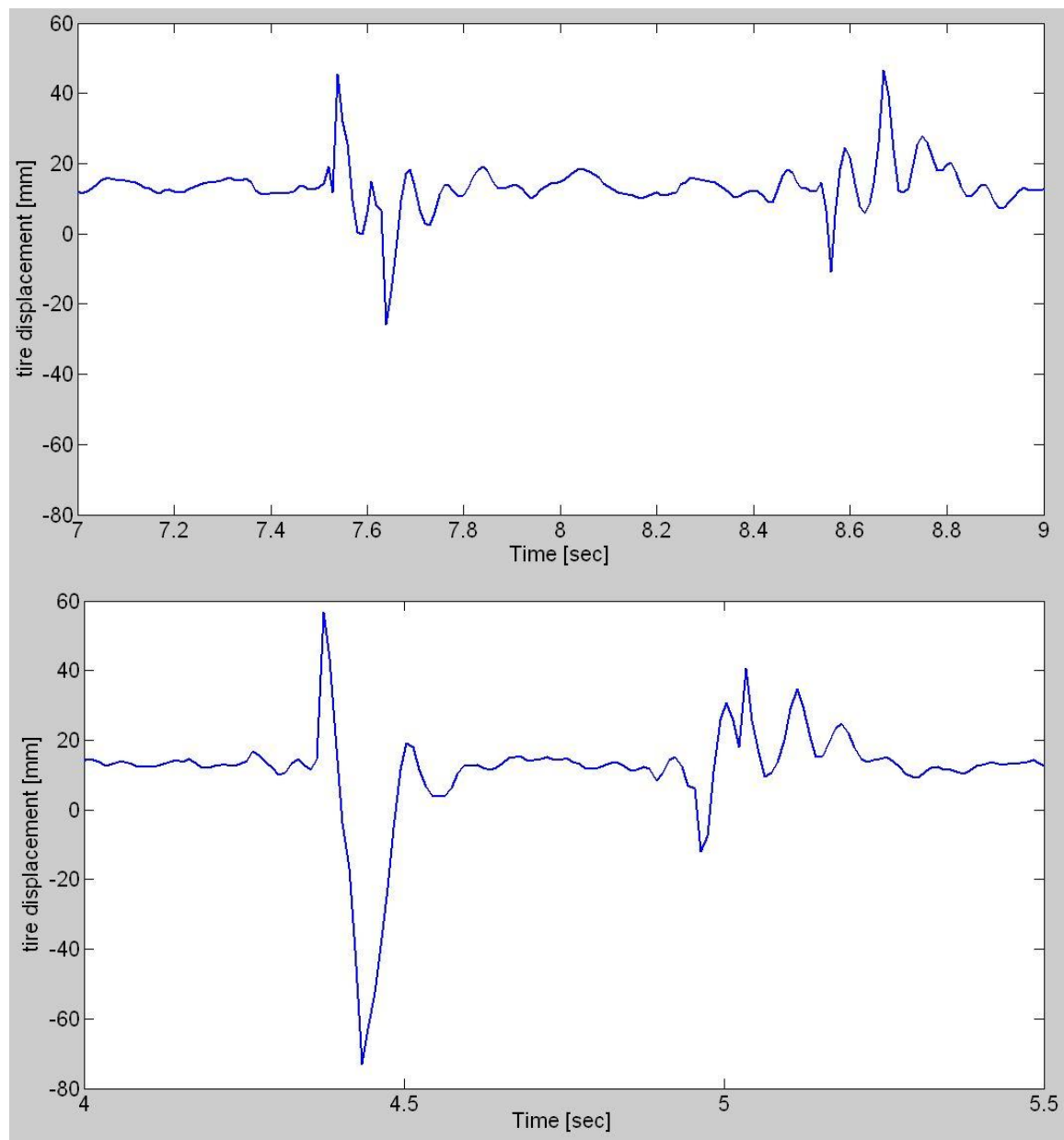


**Figure 17: Front left tire deflection, low-speed case (top) and high-speed case (bottom)**

Figure 18 shows the effect of the transverse spatial correlation of the road profile on the HMMWV FLSS joint forces at the LCA rear bushing connection. Two extreme situations of high and low spatial correlations were considered. No road curves or topography effects were included.

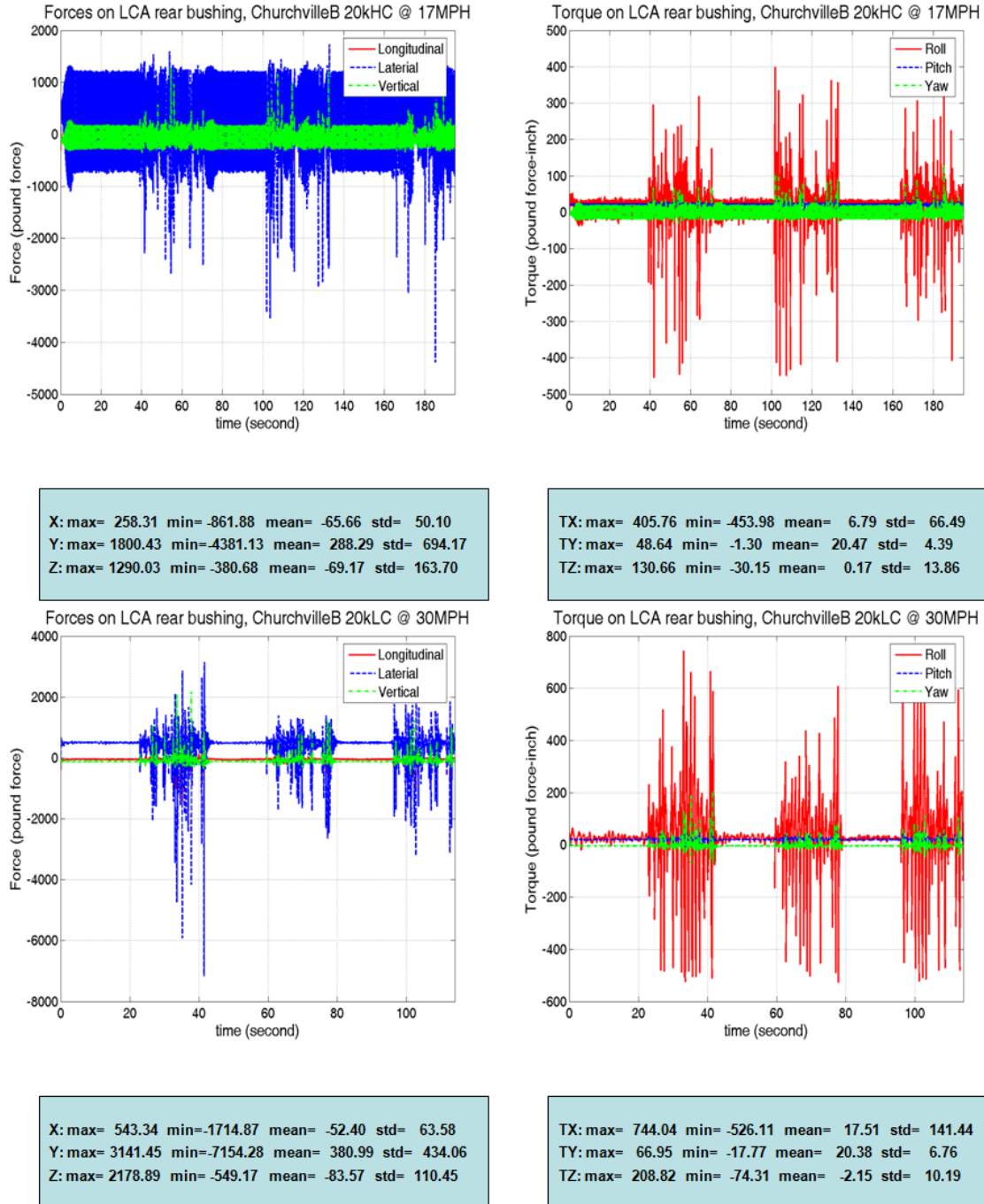


Figure 18: LCA bushing joint forces at 30MPH for high (top) and low (bottom) transverse spatial correlations

The significant amplification effect of topography on the suspension component force cycles is shown in Figure 19. This significantly affects the suspension component fatigue life that is sensitive to stress cycle ranges.



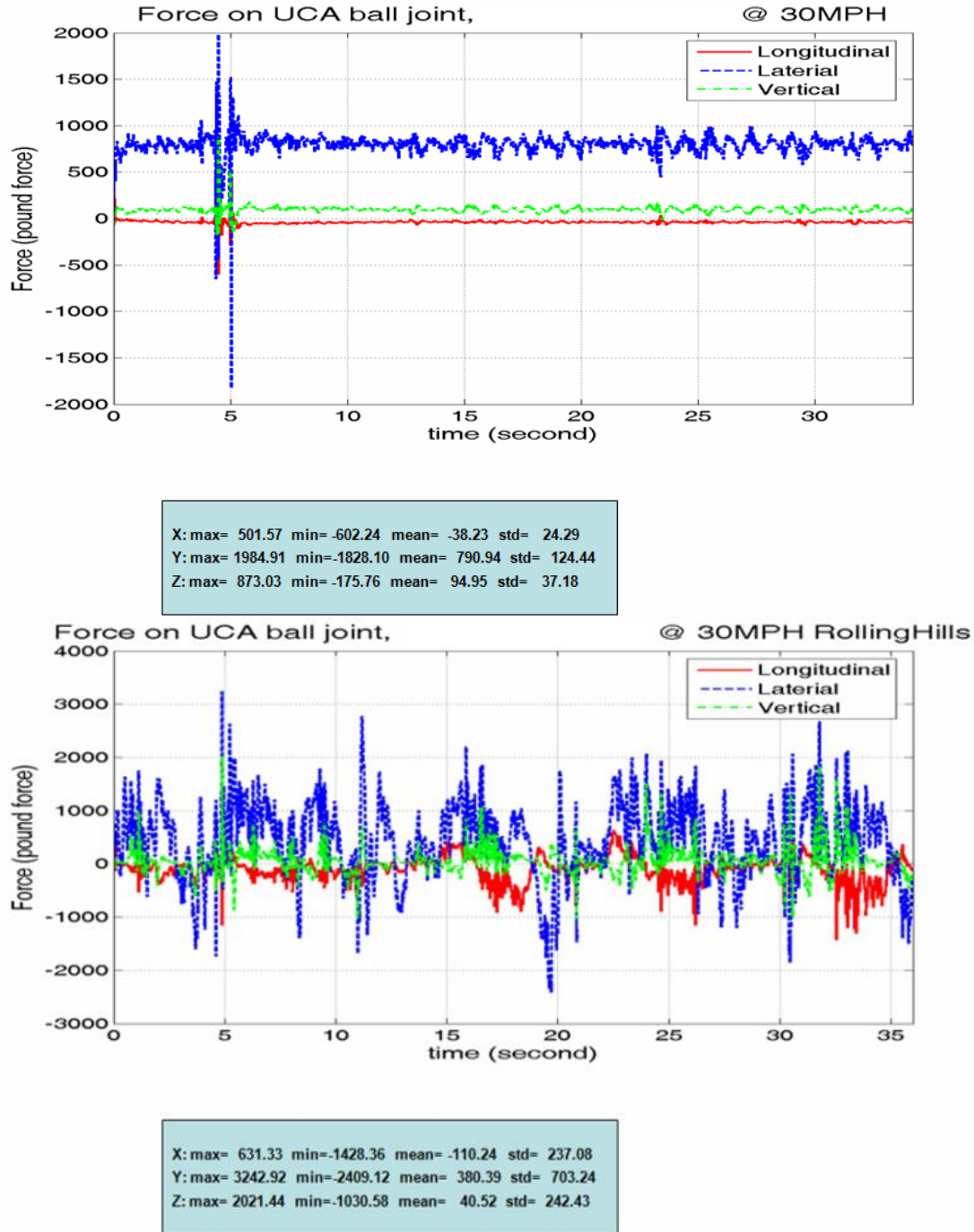
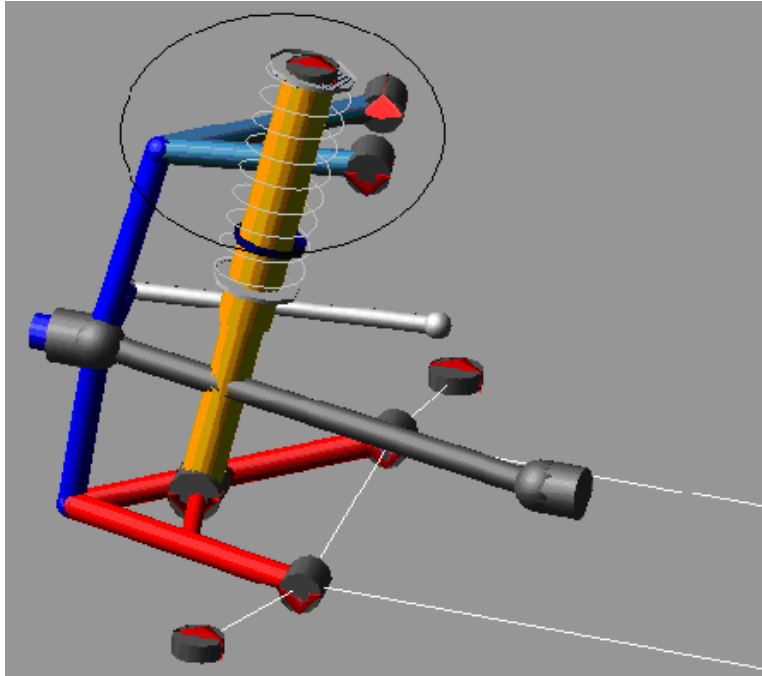


Figure 19: Effects of road topography on joint forces in front-left LCA

## 5.2 Stochastic FE Stress Analysis for Left-Front Suspension Subsystem

The selected subsystem for stochastic FE stress analysis was the vehicle Front-Left Suspension System (FLSS). Figure 20 shows the FLSS model used for the vehicle multi-body dynamics analysis and Figure 21 shows the stochastic FEA model using the FEA code.



**Figure 20: Front-left suspension system; vehicle simulation software model**

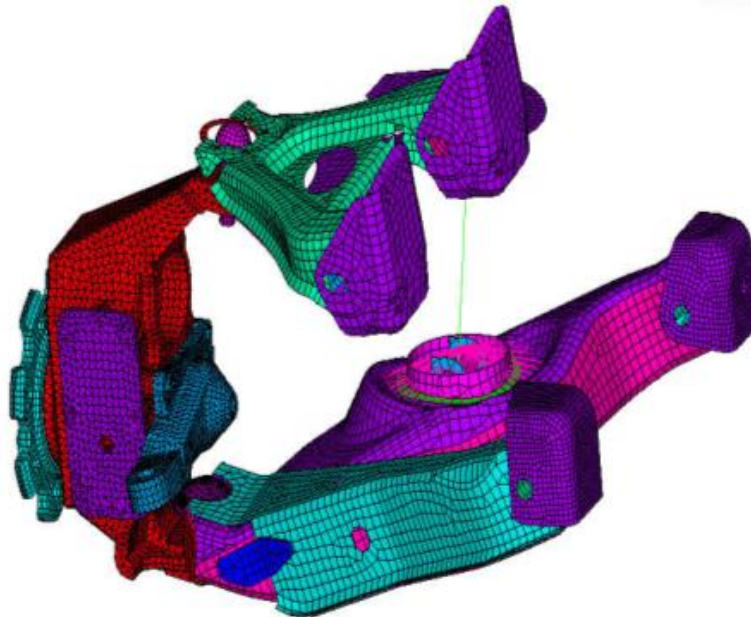


**Figure 21: Front-left suspension system; FEA model**

Vehicle parameters were also assumed to be random variables. There are a total of 13 considered random variables for each suspension unit, totaling 52 variables for the entire vehicle. To handle the large numbers of random variables, they are condensed into four stochastic variation features:

1. Upper control arm bushings (4 variables)
2. Lower control arm bushings (4 variables)

3. Tire parameters (3 variables), and
4. Shock absorber (2 variables)

The above variation features will be applied to the FLSS or all four suspension units.

From each of the vehicle dynamics simulations, we saved 34 output variables with 1-3 component time-histories for various front-left suspension joint forces and displacements, vehicle chassis motion, displacements at the wheel tire/road interface. The total number of saved component time histories per each HMMWV simulation is 94.

Out of the 94 saved component variables, 36 variables are used as inputs to the stochastic FE stress analysis of FLSS. Each joint force component was used to scale the local stress influence coefficients computed for unit forces in the joints.

### **5.3 Stochastic Life Prediction**

The linear damage rule (LDR) provides a life that is twice as long than the predicted life using a nonlinear damage rule such the damage curve approach (DCA). These results show that the unconditional use of LDR for any fatigue damage modeling could produce crude reliability analysis results.

Figure 22 shows results the probabilistic predicted life at a critical location in FLSS using the LDR and the DCA progressive damage models combined with modified stochastic Forman model [8].

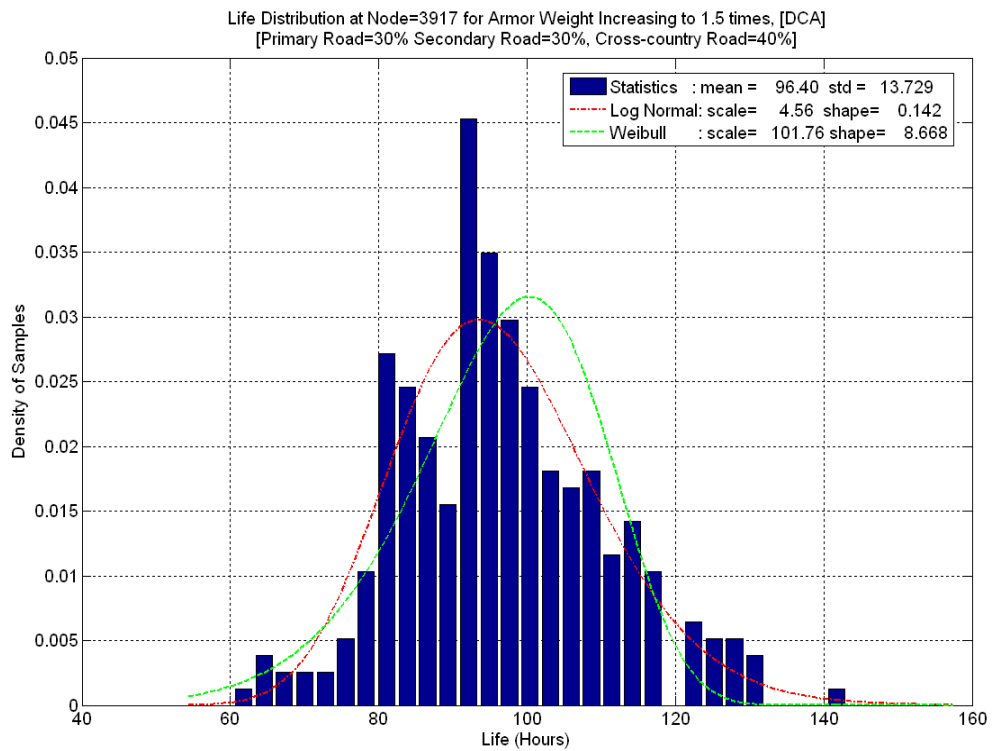
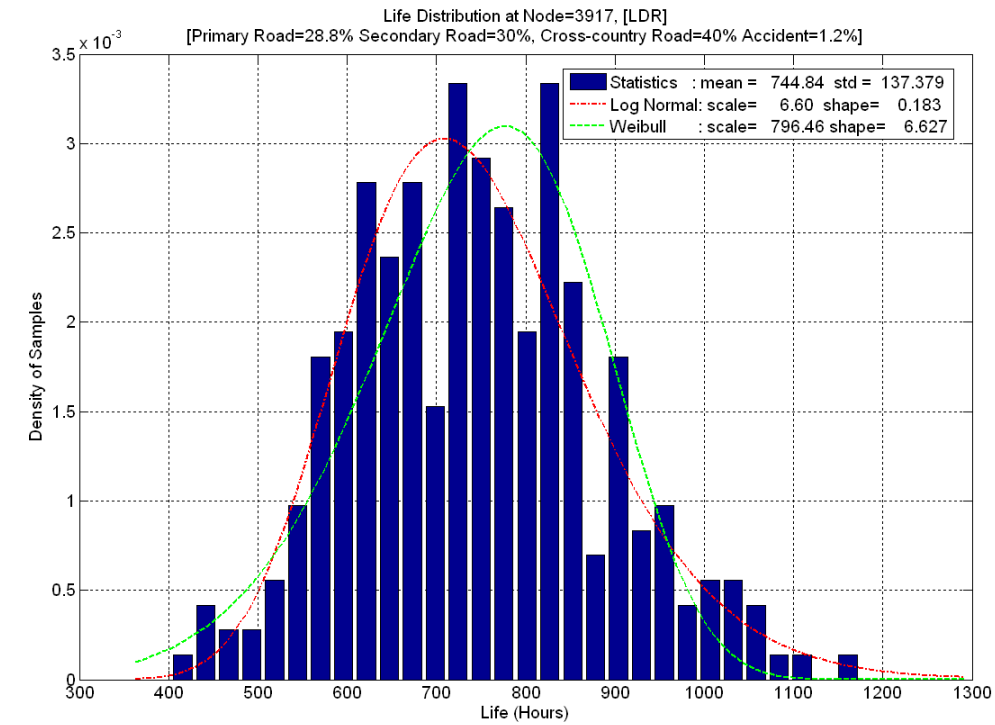


Figure 22: Predicted fatigue life in a FLSS critical location using LDR and DCA progressive damage models

Figures 23 and 24 show the effect of lack of data (280 simulations) on the probabilistic life and reliability prediction at a critical location of FLSS [1].

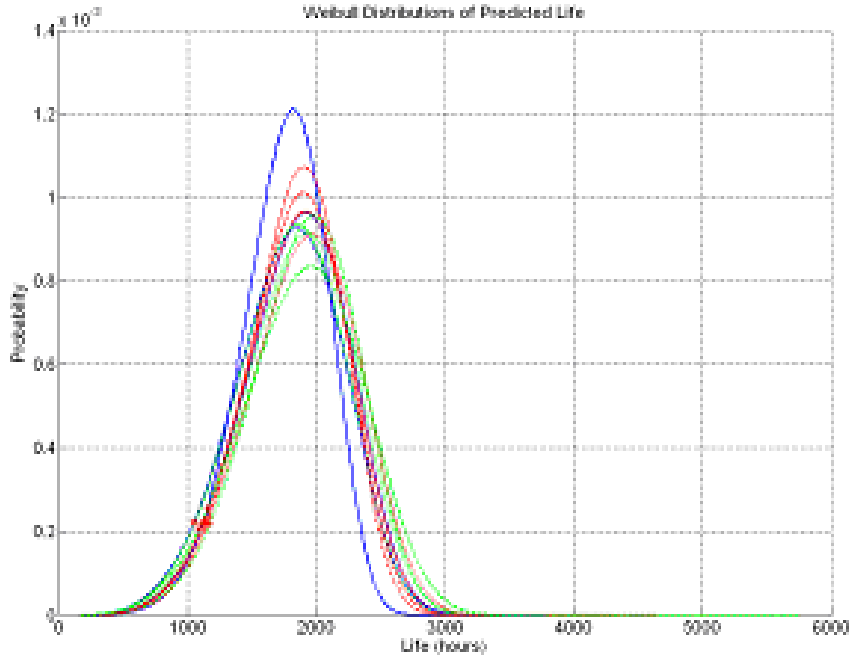


Figure 23: Predicted fatigue life in a FLSS critical location using LDR and DCA progressive damage models

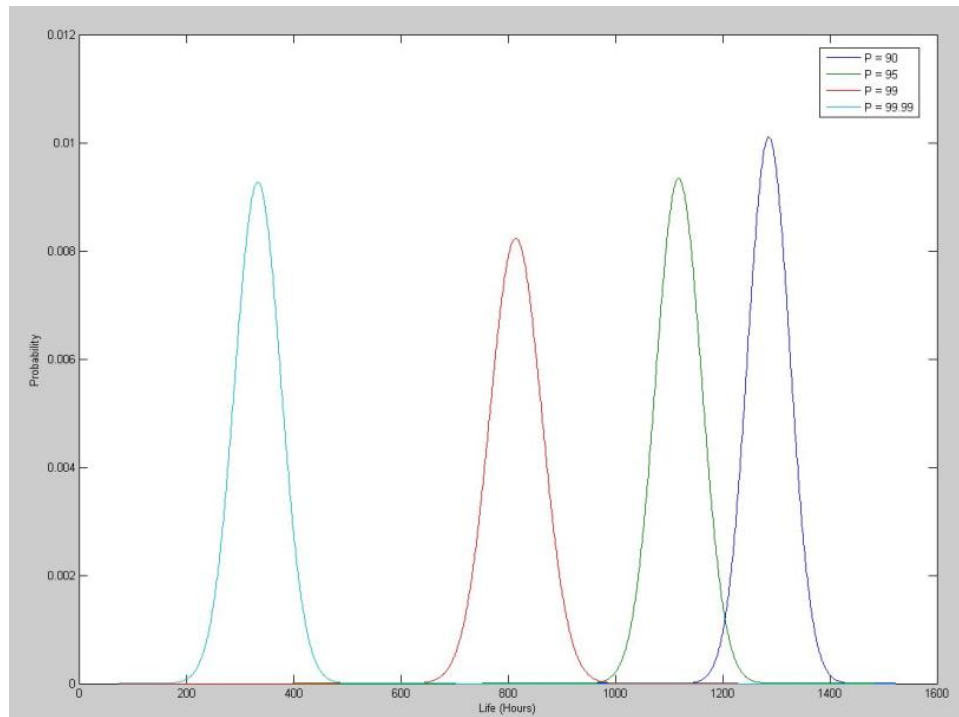


Figure 24: Effect of lack of data (280 simulations) on predicted life for given reliability levels of 90%, 95%, 99%, and 99.99%

## 6. Conclusions

Vehicle responses to stochastic model parameters and operating conditions have been simulated in a co-simulation environment using a multi-body dynamic model of the Army's HMMWV in conjunction with a high-fidelity tire model. The dynamic response of the subsystems is used as an input into a FEA to determine local stresses on the component level. Stochastic stress loading cycles serve as an input into the stochastic progressive damage models which can ultimately be used for a reliability prediction of a component or the system.

Stochastic modeling of the operating conditions included variations in height and topography of the road profiles. Road surface variation was shown to be non-Gaussian being right-skewed in the direction of larger amplitudes. Vehicle chassis velocity and the inherent randomness of a particular driver's trajectory were also treated as stochastic variables. A representative HMMWV and tire model were created, and various tire and suspension component parameters were varied.

Sample results from vehicle dynamics simulations are presented and discussed, with an emphasis on the effects of the varied road and vehicle parameters on the response. Stochastic FE stress analysis results are analyzed, with comments on the choice of a damage rule and its effect on suspension system component life predictions.

## 7. Acknowledgements

The authors would like to thank Hammad Mazhar for his assistance providing feedback on the paper. We also acknowledge the DOD SBIR funding support for GP Technologies, Inc. and University of Wisconsin -Madison under the DOD A06-224 topic.

## 8. References

- [1] Ghiocel, D.M., Lamb, D. and Hudas, G., 2007. "Advances in Computational Stochastic Mechanics and Reliability Prediction for Ground Vehicles", 2007 SIAM Conference "Mathematics for Industry", Minisymposium on Computational Reliability and Safety Simulations for Ground Vehicles, October
- [2] Aardema, J., 1988. Failure analysis of the lower rear ball joint on the High-Mobility Multipurpose Wheeled Vehicle. U.S. Army Tank-Automotive Command Technical Report # 13337, Warren, MI, August.
- [3] Frame, E., Blanks, M., 2004. Emissions from a 6.5L HMMWV engine on low sulfur diesel fuel and JP-8. U.S Army TARDEC Interim Report TFLRF No. 376, Warren, MI, December.
- [4] Gipser, M., 2005. "FTire: a physically based application-oriented tyre model for use with detailed MBS and finite-element suspension models." *Vehicle Systems Dynamics* 43(Supplement/2005), pp. 76 - 91.
- [5] Datar, M., 2007. Technical Report on Virtual Prototyping of Ground Vehicles. TR-2007-03, Simulation Based Engineering Lab - University of Wisconsin, Madison, WI.
- [6] Ghiocel, D.M., 2004. "Stochastic Simulation Methods for Engineering Predictions". In *Engineering Design Reliability Handbook*, 1<sup>st</sup> ed., Nikolaidis, Ghiocel and Singhal, eds., CRC Press, December, Chapter 20.
- [7] Ghiocel, D. M., 2005. "Advances in Computational Risk Predictions for Complex, Large Size Structural Engineering Applications" 46th AIAA/ASME/ASCE

/AHS/ASC Structures, Structural Dynamics & Material Conference, AIAA-2005-2222, Austin, TX, April 18-21.

- [8] Ghiocel, D.M., Tuegel, E., 2007. "Reliability Assessment of Aircraft Structure Joints Under Corrosion-Fatigue Damage". In *Engineering Design Reliability Applications: For the Aerospace, Automotive and Ship Industries*, 1<sup>st</sup> ed., Nikolaidis, Ghiocel and Singhal, eds., CRC Press, September.